A method to estimate the spatial coherence of photoacoustic channel data without access to channel data

Kelley M. Kempski[1], Mardava R. Gubbi[2], and Muyinatu A. Lediju Bell[1,2,3]
[1]*Department of Biomedical Engineering, Johns Hopkins University, Baltimore, MD, United States*
[2]*Department of Electrical and Computer Engineering, Johns Hopkins University, Baltimore, MD, United States*
[3]*Department of Computer Science, Johns Hopkins University, Baltimore, MD, United States*

***Abstract*—Channel signal-to-noise ratio (SNR) is a metric to assess photoacoustic image quality based on the raw photoacoustic channel data. Current methods for measuring channel SNR require access to raw data or delay data prior to summation (e.g., prior to DAS beamforming) in addition to knowledge of the noise profile to differentiate signal from noise. However, access to pre-beamformed data is not always feasible with clinical ultrasound scanners, and knowledge of noise profiles are typically not available. This paper introduces a new method for calculating channel SNR based on the probability density functions (PDFs) of beamformed data and shows how this method is related to not only channel SNR, but also other properties of channel data and image data for photoacoustic images.**

***Index Terms*—Photoacoustic imaging, raw data, image quality, coherence**

I. Introduction

Photoacoustic imaging involves the irradiation of a target using nonionizing radiation. Optical absorption of the target results in thermal expansion and the subsequent generation of an acoustic pressure wave that can be received by an ultrasound transducer [1], [2]. In more realistic clinical situations, low laser energies or tissue obstructions may result in noisy, low-quality images that are difficult to interpret [3], [4]. Assessing image quality is of critical importance. One approach to assess image quality is to be aware of the channel signal-to-noise ratio (SNR).

There are at least two widely accepted methods to measure channel SNR, which is defined as the ratio of the mean power of the signal to the mean power of the uncorrelated noise. The first method includes using the root mean square of the uncorrupted channel data over the standard deviation of the corrupted noise [5]. The second method includes measuring the signal and noise from the delayed data prior to any summation.

One limitation of relying on real-time measurements of channel SNR to assess application-specific image quality is that clinical and pre-clinical photoacoustic systems do not provide access to pre-beamformed data (i.e., raw channel data or delayed data) or noise profiles. Instead, access to beamformed images is typically the only option provided. Without access to pre-beamformed data, clinicians and investigators are unable to measure channel SNR using currently available methods.

This paper introduces a third method for calculating channel SNR based on the target and background regions of interest (ROIs) of beamformed data and shows how this method is related to not only channel SNR, but also other properties of channel data and image data for photoacoustic images. The additional properties that we will present are two recently introduced methods to assess image quality: (1) the generalized contrast-to-noise ratio (gCNR) [6], [7] and (2) lag-one coherence (LOC) [8].

II. Materials and Methods

A. Simulation methods

Photoacoustic channel data were simulated using k-Wave [5]. The transducer was defined with 0.3 mm pitch, 0.06 mm kerf, and 128 elements. A 1 mm- and 2 mm-diameter circular target containing randomly distributed optical absorbers were placed at the center of a 23.1 mm $\times$ 38.4 mm phantom.

B. Experimental methods

To create experimental data containing two different target sizes, either a 1 mm- or 2 mm-diameter fiber bundle was inserted in a plastisol phantom, and the tip of the fiber bundle was the image target. A total of ten photoacoustic images were acquired per image target using a Phocus Mobile laser (OPOTEK, Carlsbad, CA) or an LS-Series Pulsed Laser Diode (Laser Components, Bedford, NH) with laser light delivered through the 1 mm or 2 mm fiber, respectively. Each laser system was connected to an Alpinion ECUBE 12R ultrasound scanner (Seoul, Korea) to create the photoacoustic imaging system. Channel data from the 1 mm- and 2 mm-diameter image targets were acquired with a 128-element Alpinion L3-8 linear transducer and a 64-element Alpinion SP1-5 phased transducer, respectively. Additional imaging parameters are listed in Table I.

C. Beamforming methods

Photoacoustic images were created from the acquired channel data using delay-and-sum (DAS) beamforming and short-lag spatial coherence (SLSC) beamforming with a lag value of $M = 1$ [9], also termed lag-1 coherence imaging. The process

TABLE I
PHOTOACOUSTIC EXPERIMENT PARAMETERS

	Target A	Target B
Fiber Diameter	1 mm	2 mm
Wavelength	750 nm	905 nm
Laser Frequency	10 Hz	20 Hz
Pulse Width	5 ns	51 ns
Laser Energy	2.3 mJ	5.8 μJ

implemented to create the lag-1 coherence images is described by the following equation:

$$\hat{R}(1) = \frac{1}{N-1}\sum_{i=1}^{N-1}\frac{\sum_{n=n_1} n_2 s_i(n)s_{i+1}(n)}{\sqrt{\sum_{n=n_1}^{n_2} s_i^2(n)\sum_{n=n_1}^{n_2} s_{i+1}^2(n)}} \quad (1)$$

where N is the number of elements in the receive aperture, $s_i(n)$ is the time-delayed, zero-mean signal received by the ith element, n is the sample depth, n_1 through n_2 defines a correlation kernel length, and $\hat{R}$ is the normalized spatial correlation of the lag-1 coherence image. Negative values were removed from the lag-1 coherence image and set to 0.

D. Image quality metrics

The generalized contrast-to-noise ratio (gCNR) was measured from DAS beamformed images using the following equation [6]:

$$gCNR = 1 - \sum_{k=0}^{N-1}\min\{h_i(x_k), h_o(x_k)\} \quad (2)$$

where h_i and h_o are the histograms associated with the target and background ROIs, respectively, and N is the number of bins centered at $\{x_0, x_1, ...x_{N-1}\}$.

Lag-1 coherence was measured as the mean signal amplitude within a region of interest in the location of the lag-1 image target.

E. Channel SNR measurements

Channel SNR was measured using the following three methods.

- **Method 1:** Channel SNR was measured using the root mean square (RMS) according to the following equations:

$$signal_1 = \sqrt{\text{mean}(X^2)} \quad (3)$$

$$noise_1 = \sqrt{\text{std}(X^2_{noisy})} \quad (4)$$

  where X is the uncorrupted, noiseless channel data, and X_{noisy} is the noisy channel data.
- **Method 2:** Channel SNR was measured using the delay data method according to the following equations:

$$signal_2 = \sqrt{\text{mean}(X^2_{noisy,1\text{ signal channel}})} \quad (5)$$

$$noise_2 = \sqrt{\text{mean}(X^2_{noisy,1\text{ noisy channel}})} \quad (6)$$

  where the signal region was isolated to pixels associated with the target within 1 channel.
- **Method 3:** Channel SNR was measured using a new method we developed based on the ROIs of the DAS beamformed images according to the following equations:

$$signal_3 = \text{mean}(X^2_{DAS,t}) \quad (7)$$

$$noise_3 = \text{mean}(X^2_{DAS,b}) \quad (8)$$

The channel SNR is calculated using the signal and noise calculated using any of the methods defined above.

$$chSNR(dB) = 10\log_{10}\left(\frac{signal}{noise}\right) \quad (9)$$

F. Noise addition

Gaussian distributed noise was added to the simulated and experimental phantom channel data. The standard deviation of the noise was computed using Method 1 to obtain images with channel SNR values in the range -40 dB to 40 dB. The channel SNR values obtained using Method 2 and Method 3 were compared to the baseline channel SNR values obtained using Method 1.

III. RESULTS AND DISCUSSION

Fig. 1 shows the channel SNR measured using Methods 2 or 3 as a function of the channel SNR generated using Method 1. While Method 1 is beneficial for generating noisy simulated and experimental data, it is an unrealistic measurement tool. Method 1 requires access to uncorrupted channel data which is not accessible in experimental settings. Methods 2 and 3 are two testable channel SNR measurement methods for experimental data. Method 2 is shown in blue, and Method 3 is shown in orange. The 1 mm targets are shown as filled markers, and the 2 mm are shown as open markers. The experimental datasets are shown with circles, and the simulated data are shown with diamonds. For both Methods 2 and 3 in each of the datasets, there is a sigmoidal curve with a linear portion and a shoulder and toe. When Method 1 was set to low channel SNRs (e.g., -40 dB), the measured channel SNR using Methods 2 or 3 is not less than approximately 0 dB. In a noisy image where the signal is indistinguishable from background, the ratio of the signal to noise would be 1, resulting in a log measure of 0 dB. There is a plateau on the right end of the curve because once we try to set a high enough channel SNR using Method 1 (e.g., 40 dB), there is virtually no noise added to the data. The maximum possible measured value is based on inherent noise in the collected data. A lower plateau for the 2 mm experimental data is observed compared to the 1 mm experimental data as a result of significantly lower laser energy (i.e., 1 mm: 2.3 mJ, 2 mm: 5.8 μJ) which has a significantly lower maximum possible signal amplitude. There is reasonable agreement between Method 2 and Method 3. This reasonable agreement, in addition to the linear trend observed in the center of the curve, indicates Method 3 is a promising method to measure channel SNR.

Fig. 2 shows the LOC as a function of the gCNR of the DAS beamformed images for the simulated and experimental images with the best fit line for the combined datasets shown

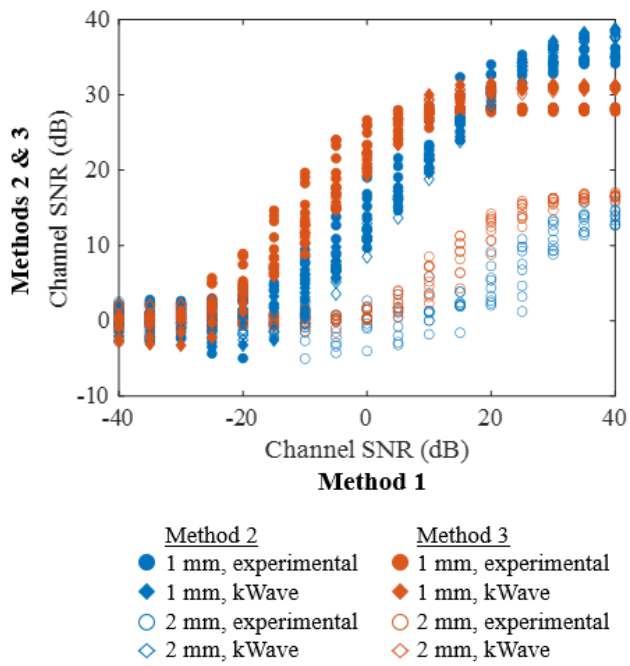

Fig. 1. Channel SNR measured using Method 2 or Method 3 as a function of channel SNR generated using Method 1 for 1 mm experimental and simulated images.

in black. The simulated datasets are represented by outlined data points and the experimental datasets are represented by filled data points. The 1 mm datasets are shown in blue and the 2 mm datasets are shown in orange. The link between each visualized data point is the channel SNR based on Method 1. For both simulated and experimental datasets, there is an exponential relationship between gCNR and LOC. There is also a correlation between the simulated and experimental datasets (i.e., R^2 = 0.8). The exponential relationship between LOC and gCNR provides the potential to predict coherence given only the DAS beamformed image. Thus, coherence information is available without requiring access to channel data. Our method of estimating channel SNR using the ROIs of DAS beamformed images produces a link from the image domain to the channel data domain. which indicates that there is a connection between LOC (which relies on channel domain data) and gCNR (which relies on image domain data).

IV. Conclusion

This work demonstrates a novel method for estimating channel SNR without access to channel data. Using the mean power ratio of the target and background ROIs of the DAS beamformed images, channel SNR can be estimated similar to channel SNR measured using delay data prior to summation. We envisage that this work will enhance the potential to provide users with the benefits of coherence information when using clinical or preclinical photoacoustic systems that do not allow access to channel data.

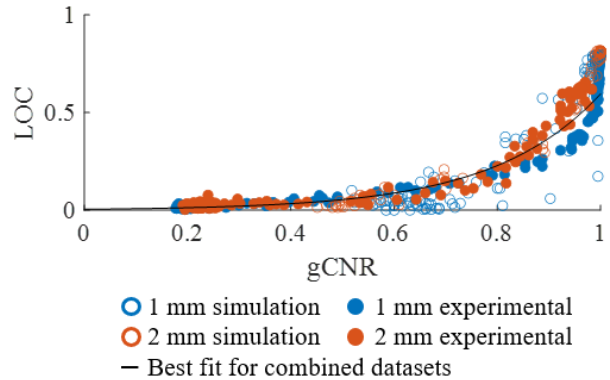

Fig. 2. LOC as a function of gCNR for the simulated and experimental phantom images.

Acknowledgments

The authors acknowledge Eduardo González for his assistance with data collection. Funding was provided by NSF CAREER Award ECCS-1751522, NSF SCH Award IIS-2014088, and in part by NSF Graduate Research Fellowship DGE1746891.

References

[1] Richard RR Bouchard, Onur Sahin, and Stanislav SY Emelianov. Ultrasound-guided photoacoustic imaging: current state and future development. *IEEE transactions on ultrasonics, ferroelectrics, and frequency control*, 61(3):450–66, 2014.

[2] Minghua Xu and Lihong V Wang. Photoacoustic imaging in biomedicine. *Review of Scientific Instruments*, 77(041101):1–22, 2006.

[3] Muyinatu A Lediju Bell. Photoacoustic imaging for surgical guidance: Principles, applications, and outlook. *Journal of applied physics*, 128(6):060904, 2020.

[4] Alycen Wiacek and Muyinatu A Lediju Bell. Photoacoustic-guided surgery from head to toe. *Biomedical Optics Express*, 12(4):2079–2117, 2021.

[5] Bradley E Treeby and Benjamin T Cox. k-wave: Matlab toolbox for the simulation and reconstruction of photoacoustic wave fields. *Journal of Biomedical Optics*, 15(2):021314, 2010.

[6] Kelley M Kempski, Michelle T Graham, Mardava R Gubbi, Theron Palmer, and Muyinatu A Lediju Bell. Application of the generalized contrast-to-noise ratio to assess photoacoustic image quality. *Biomedical Optics Express*, 11(7):3684–3698, 2020.

[7] Alfonso Rodriguez-Molares, Ole Marius Hoel Rindal, Jan D'hooge, Svein-Erik Måsøy, Andreas Austeng, Muyinatu A Lediju Bell, and Hans Torp. The generalized contrast-to-noise ratio: a formal definition for lesion detectability. *IEEE Transactions on Ultrasonics, Ferroelectrics, and Frequency Control*, 67(4):745–759, 2020.

[8] Will Long, Nick Bottenus, and Gregg E Trahey. Lag-one coherence as a metric for ultrasonic image quality. *IEEE Transactions on Ultrasonics, Ferroelectrics, and Frequency Control*, 65(10):1768–1780, 2018.

[9] Michelle T Graham and Muyinatu A Lediju Bell. Photoacoustic spatial coherence theory and applications to coherence-based image contrast and resolution. *IEEE Transactions on Ultrasonics, Ferroelectrics, and Frequency Control*, 67(10):2069–2084, 2020.